



Ca²⁺-based allosteric switches and shape shifting in RGLG1 VWA domain

Qin Wang^{a,d}, YaYu Chen^b, ShengPing Li^c, WenDi Yang^b, LiFang Sun^b, MeiQin Jang^a,
XiuLing Wu^a, QianChao Wang^a, Lifei Chen^b, YunKun Wu^{b,*}

^a State Key Laboratory of Structural Chemistry, Fujian Institute of Research on the Structure of Matter, Chinese Academy of Sciences, 155 Yangqiao West Road, Fuzhou 350002, China

^b Provincial University Key Laboratory of Cellular Stress Response and Metabolic Regulation, College of Life Science, Fujian Normal University, Fuzhou 350117, China

^c Key Laboratory of Ministry of Education for Genetics, Breeding and Multiple Utilization of Crops, Plant Immunity Center, Fujian Agriculture and Forestry University, Fuzhou 350002 China

^d University of Chinese Academy of Sciences, Beijing 100049, China

ARTICLE INFO

Article history:

Received 10 October 2019

Received in revised form 24 March 2020

Accepted 25 March 2020

Available online 30 March 2020

Keywords:

VWA domain

Open state

Closed state

Calcium ions binding site

Conformational change

Molecular dynamics simulation

ABSTRACT

RGLG1 is an E3 ubiquitin ligase in *Arabidopsis thaliana* that participates in ABA signaling and regulates apical dominance. Here, we present crystal structures of RGLG1 VWA domain, revealing two novel calcium ions binding sites (NCBS1 and NCBS2). Furthermore, the structures with guided mutagenesis in NCBS1 prove that Ca²⁺ ions play important roles in controlling conformational change of VWA, which is stabilized in open state with Ca²⁺ bound and converted to closed state after Ca²⁺ removal. This allosteric regulation mechanism is distinct from the ever reported one involving the C-terminal helix in integrin α and β I domains. The mutation of a key residue in NCBS2 do not abolish its Ca²⁺-binding potential, with no conformational change. MD simulations reveals that open state of RGLG1 VWA has higher ligand affinity than its closed state, consisting with integrin. Structural comparison of ion-free-MIDAS with Mg²⁺-MIDAS reveals that Mg²⁺ binding to MIDAS does not induce conformational change. With acquisition of first structure of plant VWA domain in both open state and closed state, we carefully analyze the conformational change and propose a totally new paradigm for its transition of open-closed states, which will be of great value for guiding future researches on VWA proteins and their important biological significance.

© 2020 The Authors. Published by Elsevier B.V. on behalf of Research Network of Computational and Structural Biotechnology. This is an open access article under the CC BY-NC-ND license (<http://creativecommons.org/licenses/by-nc-nd/4.0/>).

1. Introduction

In *Arabidopsis thaliana*, RGLG1 (RING domain ligase 1) is a RING-type E3 ubiquitin ligase that belongs to the RGLG family, and the four additional members are named RGLG 2 to 5. RGLG1 contains a Von Willebrand factor A (VWA) domain at the center and a really interesting new gene (RING) domain at the C-terminal region [1]. It can be anchored to the plasma membrane by myristoylated Gly2, although it does not contain a transmembrane domain [1].

RGLG1 and its homolog RGLG2 play important roles in regulating auxin and cytokinin levels [1]. Numerous plant traits influenced by auxins can be changed through inactivation of both RGLG1 and RGLG2, e.g., abolishing apical dominance and altering normal leaf phyllotaxy. However, the effect of single *rglg1* or *rglg2* mutants are inconspicuous [1]. *Rglg1* and *rglg2* mutations alters the expression of genes regulated by cytokinin and auxin levels, e.g., cytokinin-responsive gene expression levels are higher in mutants

than in wild type, whereas the auxin-responsive gene expression levels are lower. Furthermore, RGLG1 and RGLG2 regulate epidermal development, and *rglg1 rglg2* mutants show a high percentage of branched root hair [2,3]. In addition, RGLG1 contributes to the abscisic acid (ABA) signaling pathway with another homologous protein RGLG5 [4]. Abscisic acid is an essential hormone for plant survival, and the type 2C protein phosphatases (PP2Cs) are critical negative regulators of the ABA signaling network [5,6]. PP2CA, a PP2Cs family member, inactivates SNF1-related protein kinase 2 (SnRK2) through dephosphorylation [6]. RGLG1 and RGLG5 can interact with PP2CA and mediate its ubiquitination for proteasome degradation *in vivo* and *in vitro* [4]. The *rglg1* and *rglg5* double mutant shows reduced survival in drought stress conditions, whereas RGLG1 or RGLG5 overexpression reduces water loss and markedly enhances plant survival. With the closest sequences, phenotypes do not change when only one of RGLG1 and RGLG5 is mutated [4]. Interestingly, interaction between RGLG1/5 and PP2CA *in vitro* do not require ABA, whereas, ABA enhances the nuclear interaction with PP2CA *in vivo* [4,7]. The fact that ABA downgrade N-myristoyltransferase 1 (NMT1) to inhibit the myris-

* Corresponding author.

E-mail address: wuyk@fjnu.edu.cn (Y. Wu).

toylation of RGLG1 and enhance its nuclear recruitment is determined by Belda-Palazon et al. [7]. Calcium ions and PP2CA protein also enhance nuclear localization of RGLG1. These evidences provide a mechanism that ABA enhances RGLG1–PP2CA interaction and hence PP2CA degradation [7]. VWA domains serve as interaction modules in many proteins, e.g., extracellular matrix proteins, integrin, and complement factors B and C2, and many human diseases result from their mutations [8]. They usually adopt a classic α/β “Rossmann” fold or a featured dinucleotide-binding conformation, which has several central β strands with one antiparallel edge sheet and several α helices around the β sheets [8]. Two terminal cysteine residues form a disulfide bridge to stabilize the domain [9]. Numerous VWA domains have an important metal-ion-dependent adhesion site (MIDAS) with three highly conserved non-contiguous elements (D-x-S/T-x-S...T...D, x represents any amino acid) playing central roles in ligand binding [10]. The three conserved elements are located in three different loops, with D-x-S/T-x-S being the first region, and the others T4 and D5, respectively. Not all VWA domains have perfect MIDAS motifs [8]. VWA domains in integrin α and β subunits (also called I domains or A domains) have two different conformations, open and closed, and α I domain has an additional intermediate conformation [10–16]. In the open conformation, corresponding to high affinity state, Mg^{2+} in the MIDAS motif has six coordination sites and forms an octahedral coordination with two serine residues of the first region, T4, two water molecules ($\omega 1$ and $\omega 2$), and a ligand or pseudo ligand [12,16]. The two aspartic acid residues occupy a secondary coordination sphere. Their carboxylate groups indirectly coordinate the metal ion by forming a $\omega 1$ -mediated hydrogen bond [17]. In the closed conformation, corresponding to low affinity state, coordination bonds with the first region are unchanged, resulting from ionic displacement in the MIDAS motif; the coordination bonds in T4 are disrupted and replaced by a direct bond with D5, and the ligand is replaced by another water molecule [11]. Furthermore, the transition between open and closed conformations of the integrin αM I domain are considered to be associated with the rearrangement of a C-terminal α helix [11,12]. This conformational change is apparently paradigmatic for VWA domains.

Two additional ion-binding sites—ADMIDAS (adjacent to MIDAS) and SyMBS (synergistic metal ion-binding site) exist in the integrin β -subunit I domains. They regulate ligand-binding affinity [18]. At a high Ca^{2+} concentration, ADMIDAS negatively regulates integrin activation [18–22]. Mutagenesis studies have reported that ADMIDAS exerting contrasting effects on ligand binding in different integrins. SyMBS positively regulates the ligand–integrin binding at low Ca^{2+} concentrations [18]. Ca^{2+} is predicted to have a higher affinity than Mg^{2+} for the SyMBS because the SyMBS has two backbone and one amide side chain carbonyl oxygen coordination, and Ca^{2+} has a far greater propensity than Mg^{2+} to form a coordination with backbone carbonyl oxygen [23,24].

The most ancient VWA-containing proteins are all intracellular proteins involved in various important physiological phenomena including transcription, membrane transport, DNA repair, and the proteasome pathway [8]. Subsequently, metazoan develop extracellular VWA proteins. However, the intracellular complement of plants expands exclusively for novel biological functions [8]. Thus far, integrin I domains are the only examples for clarifying the mechanism of VWA conformational changes. Many other VWA proteins including C2a and factor B, the anthrax receptor, and Ro, only have the open conformation, and closed conformation has not yet been resolved. With low sequence homology among integrin and plant VWA, different allosteric regulation mechanisms may mediate transitions in the open and closed conformations. Therefore, more structures for both the open and closed state of VWA proteins are crucial to decipher the different mechanism.

This study firstly reports the crystal structures of the plant VWA domain with two different conformations and shows novel paradigms for conformational changes. In the RGLG1 VWA domain, two unexpected Ca^{2+} -binding sites have been determined. Furthermore, removing Ca^{2+} from NCBS1 successfully cause the corresponding allosteric switches, thus revealing the mechanism of conformational changes distinct from integrins, and facilitating future studies on VWA-containing proteins.

2. Results

2.1. Overall structure of the RGLG1 VWA domain

The crystal structure of the RGLG1¹²⁹ (residues R129–Q410) was resolved via selenomethionyl single-wavelength anomalous dispersion phasing at 2.2 Å resolution, containing all residues of the VWA domain (N156–L376). Crystals grew in space group P41, with two molecules per asymmetric unit. Data collection and refinement statistics are summarized in Table 1. Similar to other members of VWA domains, the RGLG1 VWA contains a typical Rossmann fold, a central five-stranded hydrophobic β sheet surrounded by nine amphipathic α helices, β sheets and α helices are labeled $\beta 1$ to $\beta 5$ and $\alpha 1$ to $\alpha 9$, respectively (Fig. 1a and b). A conserved MIDAS motif located at the top face comprises a DxTxS sequence (residues 162–166) from the $\beta 1$ - $\alpha 2$ loop and $\alpha 2$ helix, T258 from the $\alpha 4$ - $\alpha 5$ loop, and D286 from the $\beta 3$ - $\alpha 6$ loop. The strong globular electron density presented at MIDAS is modelled as a Mg^{2+} ion, since it is the only metal ion in the crystallization buffer, and distinguished from water in accordance with bond lengths and octahedral coordination. Mg^{2+} is coordinated by hydroxyl groups of MIDAS residues T164, S166, T258, and two water molecules, a carboxylate oxygen from E153 of the neighboring domain serving as a pseudo ligand to complete the octahedral coordination. D162 and D286 indirectly coordinate Mg^{2+} by forming hydrogen bonds with one water molecule (Fig. 1). Compared with the conformation of the MIDAS residues in integrin αM I domain, we determined that RGLG1¹²⁹ assumed an open conformation [12]. Unlike numerous VWA domains, RGLG1¹²⁹ is devoid of an intramolecular disulfide bond between the N- and C-termini that stabilize the structure [9,12]. In addition, a ubiquitous anti-parallel β sheet is also absent in the RGLG1¹²⁹ structure [12,25–27] (Supplementary Fig. 1).

2.2. Two novel Ca^{2+} binding sites

Distinct from other VWA domains, two Ca^{2+} binding sites are present in RGLG1¹²⁹, one located between $\alpha 7$ and $\alpha 9$ bound with two Ca^{2+} ions is termed novel calcium ion binding site 1 (NCBS1) and two Ca^{2+} ions are termed Ca1 and Ca2 (Fig. 2a and b). The other site at the bottom face, binding one Ca^{2+} ion, is termed NCBS2 (Fig. 2c). All three Ca^{2+} ions adopt pentagonal bipyramidal coordination, with seven coordinating ligands, and the Ca^{2+} -O bond distances are approximately 2.4 Å. Coordination motifs are shown in Table 2. The coordination stereochemistry confirmed the excess electron densities at NCBS1/2 as Ca^{2+} .

ADMIDAS and SyMBS are two Ca^{2+} binding sites in the integrin β I domain, however, they are significantly different from NCBS1/2. In the integrin β I domain, three ion binding sites form an inter-linked linear array, MIDAS occupying the central position and flanked by ADMIDAS and SyMBS [18]. In RGLG1¹²⁹, NCBS1/2 are distant from MIDAS, NCBS1 located at the flank and NCBS2 present almost opposite to MIDAS. In addition, the coordination motifs are different. Ca^{2+} in ADMIDAS exhibited distinct coordination bonds in different conformations, e.g., in the closed state of $\alpha 5\beta 1$, Ca^{2+} adopt the pentagonal bipyramidal, forming seven coordinate

Table 1
Data collection and refinement statistics.

Property	RGLG1 ¹²⁹	RGLG1 ^{open-H₂O}	RGLG1-Ca ²⁺	RGLG1 ^{E378A}	RGLG1 ^{D338A}	RGLG1 ^{D338A/E378A}	RGLG1 ^{EGTA}	RGLG1 ^{closed-H₂O}	RGLG1 ^{D207G}	
Space group	P 41	P 41	P 21 21 21	P 21 21 21	P 21 21 21	P 21 21 21	P 21 21 21	P 21 21 21	P 1 21 1	
Cell constants a, b, c, α, β, γ	136.18 Å 136.18 Å 56.86 Å 90.00° 90.00° 90.00°	136.28 Å 136.28 Å 55.37 Å 90.00° 90.00° 90.00°	42.88 Å 70.73 Å 146.40 Å 90.00° 90.00° 90.00°	45.59 Å 72.56 Å 80.85 Å 90.00° 90.00°	45.69 Å 72.87 Å 79.44 Å 90.00° 90.00°	44.45 Å 73.33 Å 82.28 Å 90.00° 90.00°	44.45 Å 73.33 Å 82.28 Å 90.00° 90.00°	45.62 Å 72.94 Å 80.08 Å 90.00° 90.00°	42.79 Å 73.69 Å 82.44 Å 90.00° 90.00°	141.12 Å 42.18 Å 243.44 Å 90.00° 91.08° 90.00°
Resolution (Å)	48.96–2.21	48.01–2.40	37.00–1.79	28.39–1.59	39.72–1.61	41.14–1.40	40.04–1.69	37.98–1.50	46.51–2.39	
Unique reflection	52,083	39,684	50,373	36,579	34,983	53,506	30,559	39,684	114,083	
% Data completeness (in resolution range)	98.9 (48.96– 2.21)	98.7 (48.01– 2.40)	94.0 (37.00– 1.79)	95.2 (28.39– 1.59)	94.2 (39.72– 1.61)	90.5 (41.14– 1.40)	99.1 (40.04– 1.69)	93.1 (37.98– 1.50)	98.5 (46.51– 2.39)	
R _{merge}	0.15	0.22	0.17	0.15	0.17	0.08	0.14	0.19	0.16	
$\langle I = \sigma(I) \rangle$	2.81 (at 2.20 Å)	1.64 (at 2.39 Å)	1.50 (at 1.78 Å)	1.02 (at 1.59 Å)	1.08 (at 1.61 Å)	1.24 (at 1.40 Å)	1.10 (at 1.69 Å)	1.14 (at 1.50 Å)	2.02 (at 2.39 Å)	
R, R _{free}	0.168, 0.190	0.187, 0.226	0.196, 0.234	0.200, 0.235	0.197, 0.224	0.200, 0.217	0.190, 0.226	0.195, 0.228	0.209, 0.265	
Wilson B-factor (Å ²)	37.2	45.1	16.9	30.5	28.6	20.1	24.5	19.7	39.2	
Bulk solvent k _{sol} (e/ Å ³), B _{sol} (Å ²)	0.34, 29.6	0.32, 29.5	0.30, 43.2	0.34, 41.9	0.34, 41.6	0.35, 37.3	0.36, 41.1	0.34, 40.2	0.33, 34.9	
Fo, Fc correlation	0.96	0.95	0.94	0.96	0.96	0.96	0.96	0.96	0.93	
Total number of atoms	4664	4510	3984	2380	2383	2472	2434	2539	17,985	
Average B, all atoms (Å ²)	41.0	50.0	22.0	38.0	32.0	25.0	28.0	23.0	43.0	
Ramachandran plot										
Favored region (%)	97.5	95.3	95.9	96.4	97.1	97.1	97.9	97.5	93.6	
Outliers (%)	0.6	0.5	0.7	0	0	0	0	0	1.3	
PDB code	6K8B	6K8A	6K88	6K86	6K85	6K82	6K89	6K87	6K83	

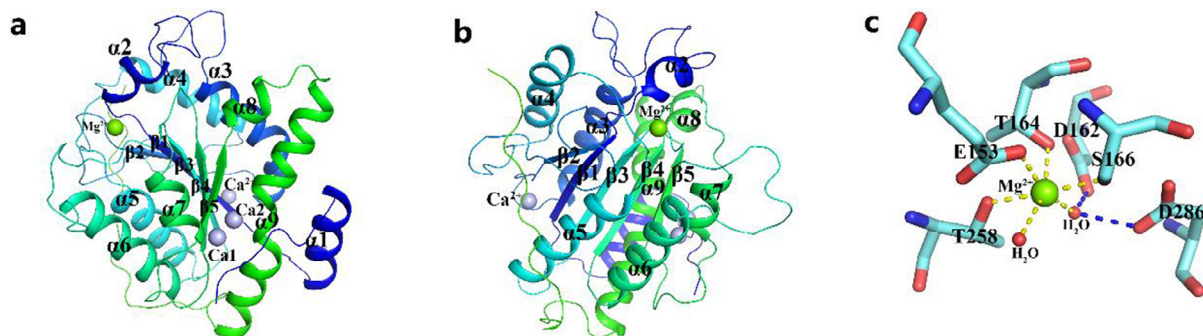


Fig. 1. Structure of the RGLG1 VWA domain. (a) Ribbon diagram of the RGLG1 VWA domain, and the α helices and β strands are labeled $\alpha 1$ to $\alpha 9$ and $\beta 1$ to $\beta 5$, respectively. The Mg^{2+} ion is shown as a chartreuse sphere, and three Ca^{2+} ions are shown as light blue spheres. (b) Same as (a) but y is rotated by 90° . (c) Stereo diagram of the MIDAS site, wherein the Mg^{2+} ion is shown as a chartreuse sphere, and two bound water molecules are depicted as small red spheres. The E153 residue from a neighboring molecule contributes the sixth coordinating residue. D286 and D162 coordinate Mg^{2+} indirectly through hydrogen bonds (the blue dotted line). (For interpretation of the references to colour in this figure legend, the reader is referred to the web version of this article.)

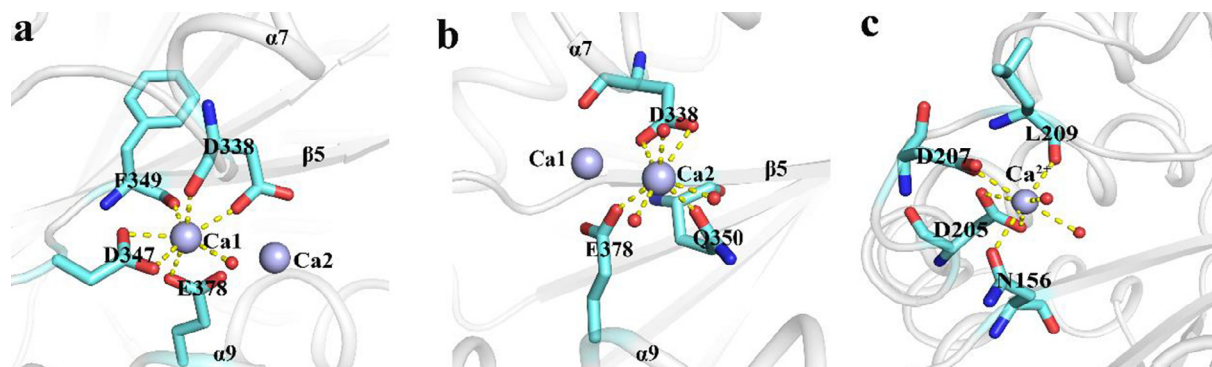


Fig. 2. Stereo diagram of NCBS1 and NCBS2. (a) The coordination residues for Ca1 (residue numbers are as indicated) are shown. The Ca^{2+} ion is depicted by a light blue sphere, and water molecules are depicted as small red spheres. (b) Ca2 is coordinated by three water molecules (small red spheres), Q350, D338, and E378. (c) Ca^{2+} ion at NCBS2 is coordinated by two water molecules, D207, D205, N156 and L209. (For interpretation of the references to colour in this figure legend, the reader is referred to the web version of this article.)

Table 2
The coordination motif of Ca²⁺.

Cation binding site	Coordination motif					
NCBS1	Ca1	bidentate carboxylate ligands of D347	monodentate carboxylate ligands of D338 and E378	main chain carbonyl oxygen atoms of F349 and D338		one water molecule
	Ca2	bidentate carboxylate ligands of D338	monodentate carboxylate ligand of E378	side chain carbonyl oxygen atom of Q350		three water molecules
NCBS2		bidentate carboxylate ligands of D205	monodentate carboxylate ligand of D207	main chain carbonyl oxygen atom of L209	side chain of N156	two water molecules

bonds with a bidentate coordination at D137, while in the open state of α IIb β 3, Ca²⁺ is more likely to form octahedral conformation, and assuming monodentate coordination with Asp [15,19]. Ca²⁺ in SyMBS adopts octahedral coordination with non-bidentate bonds in both closed and open states of integrin α 5 β 1 [28]. While NCBS1 and NCBS2 form pentagonal bipyramidal and bidentate coordination regardless of the conformation.

2.3. Conformational changes due to Ca²⁺ removal from NCBS1

To investigate whether mutations at key residues in NCBS1 impedes Ca²⁺ binding, the crystal structures of the D338A, E378A, and D338A/E378A mutants of RGLG1 were determined. All structures of mutants present one molecule in an asymmetric unit and they are nearly identical, however, these structures exhibit obvious differences from the open conformation. Mutants inhibit Ca²⁺ binding and result in a 22° sideways shift in α 7 (Fig. 3a). The side chain of D338, which interacts with two Ca²⁺ ions, points away from NCBS1 and moves 3.8 Å (Fig. 3b). The side chain of E378, which also coordinates two Ca²⁺ ions, rotates by 90° (Fig. 3c). Furthermore, one major difference is that α 1 shifts outward, almost parallel to α 9 (Fig. 3a). In the MIDAS motif, Mg²⁺ moves toward α 3 by 1.8 Å, which inhibits it from binding simultaneously with S166 and T258, resulting in a carbonyl oxygen of D286 replace T258 to directly coordinate Mg²⁺ (Fig. 3d and e). Therefore, Mg²⁺ is coordinated by T164, S166, D286, and three water molecules in mutant structures (Fig. 3d). A comparison of the MIDAS motif between these structures and that of the integrin α M I domain indicates that all mutants crystallized in the closed conformation [11], revealing that NCBS1 mutations are associated with structural transition from the open to closed conformation.

Moreover, RGLG1^{EGTA} has been crystallized in the closed conformation with the purification buffer was supplemented with 2 mM EGTA to eliminate calcium ions. Comparison of RGLG1^{EGTA} and RGLG1^{E378A} displays a root-mean-square deviation (RMSD) of 0.19 Å² (Fig. 3f), implying that direct elimination of Ca²⁺ from NCBS1 can also induce conformational changes. The present results indicate that NCBS1 is an allosteric regulatory site in the RGLG1 VWA domain, displaying a strong correlation between Ca²⁺ and the conformational state. On binding with Ca²⁺, the structure is stabilized in the open conformation; however, upon Ca²⁺ depletion, the domain converts to the closed conformation.

In α -integrin I domains, the process of conformational conversion to the closed state are conservative. A C-terminal conserved Ile residue inserts into hydrophobic pocket II, and the C-terminal helix moves 10 Å up. These changes are associated with burial of a conserved Phe residue to hydrophobic pocket I. Then a second Phe residue has backbone flip so that causing shift in the carbonyl of Gly243 and its α C [25,26]. Our structural changing mechanism is apparently distinct from that of the integrin α I domain, lacking the first Phe residue and movement of the C-terminal helix, while Gly

(287) is highly conserved. In RGLG1 VWA, the α 7 helix may correspond to the integrin α I C-terminal helix, and the substitute for the second Phe is Trp (331) located at α 7- β 4 loop. Elimination of Ca²⁺ from NCBS1 via mutations or EGTA results in a shift of α 7, then the phenylindole ring of W331 moves 2.2 Å closer to the α 6- β 3 loop, and causes a movement in the α C of G287 by 2.8 Å and the carbonyl group of G287 rotates by 90°. Thereafter, side chain of D286 shifted by 2.1 Å, facilitating direct linkage with Mg²⁺ (Fig. 3g). A water molecule replaces the pseudo ligand to complete the coordination, and conformation is converted to closed state. This Ca²⁺-dependent RGLG1 VWA conformation shows that the mechanism for transition of open-closed states is different from integrins.

2.4. NCBS2 mutation has no effects on conformational changes

Since NCBS1 is the allosteric regulatory site of RGLG1 VWA, is NCBS2 the same? Thus the mutations D205A and D207G were evaluated, and we find that the D207G mutation in NCBS2 did not affect conformational conversion. The crystal structure of RGLG1^{D207G} was resolved using molecular replacement in PHASER (Table 1). RGLG1^{D207G} does not lose its binding potential for Ca²⁺ and does not influence conformation. However, the mutation disrupts Ca²⁺ coordinate bonds, and the coordination geometry is changed from pentagonal bipyramidal to octahedral coordination (Fig. 4a and b). The structure of D205 mutant cannot be obtained owing to poor electron density. In all closed conformations, NCBS2 binds Na⁺ (Fig. 4c), except that RGLG1^{D338A} binds Mg²⁺ (Fig. 4d). The Na⁺ ion has six ligands: three ligands are hydroxyl oxygen atoms of D205, D207, and N156, and three are water molecules (Fig. 4c). In RGLG1^{D338A}, the shift of Mg²⁺ away from N156 alters its coordination: a water molecule replaces N156 to bind Mg²⁺ (Fig. 4e); therefore, Mg²⁺ in NCBS2 is coordinated by D205, D207, and four water molecules (Fig. 4d). Our hypothesis that the reason of the D207G mutation does not influence conformation was that Ca²⁺ could not be deprived, since NCBS2 binds Ca²⁺ in all open states but loses Ca²⁺ in all closed states. NCBS2-bound Ca²⁺ potentially contributes to conformational stability; however, further studies are required to characterize the underlying mechanisms.

2.5. Structure of Ca²⁺ bound MIDAS

RGLG1-Ca²⁺, containing residues S155-P380, was resolved at 1.8 Å resolution through molecular replacement, considering RGLG1¹²⁹ as a reference model (Table 1). Two molecules are present in an asymmetric unit. The structure adopts an open conformation with a Ca²⁺ ion occupying MIDAS (Fig. 5a). RGLG1-Ca²⁺ was remarkably similar to RGLG1¹²⁹, presenting an RMSD of merely 0.57 Å for all C α atoms, and exhibiting highly similar in MIDAS (Fig. 5c). However, instead of E153, E296 of the neighboring molecule serves as a pseudo ligand (Fig. 5a). Direct contact

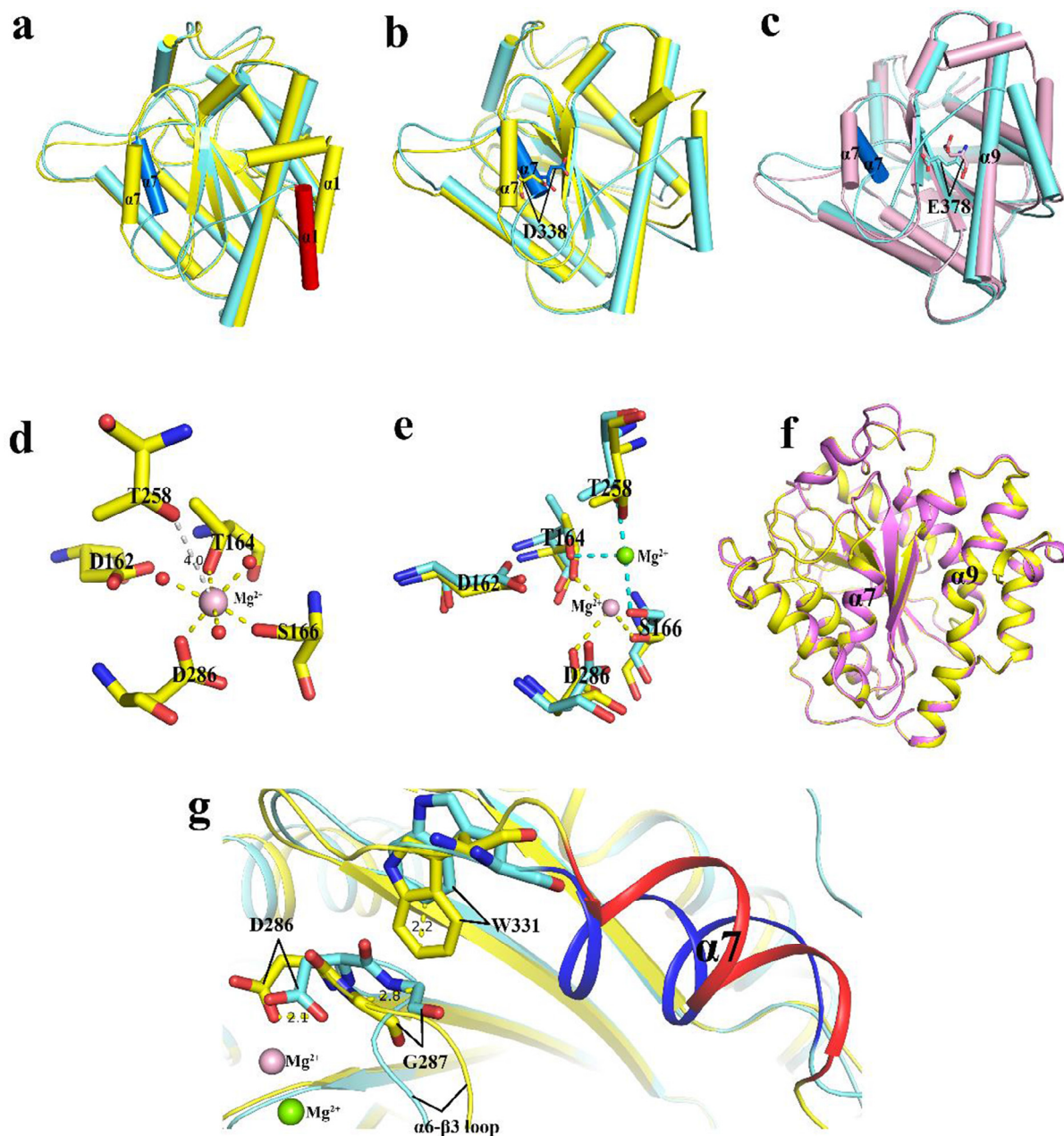


Fig. 3. Comparison of the open and closed conformations of RGLG1 VWA. (a) Comparison between open conformation (aquamarine) and closed conformation (yellow), apparently movements occur in $\alpha 1$ and $\alpha 7$. In the open conformation, $\alpha 7$ helix is highlighted in blue; $\alpha 1$ helix, red. (b) Compared with RGLG1¹²⁹ (aquamarine), D338 in the RGLG1^{E378A} (yellow) moves 3.8 Å. (c) Compared with RGLG1¹²⁹ (aquamarine), the side chain of E378 in the RGLG1^{D338A} (little pink) rotates $\sim 90^\circ$. (d) Coordination residues for Mg^{2+} (little pink sphere) in the closed conformation are as indicated. Water molecules are shown as small red spheres. The direct coordination between T258 and Mg^{2+} is destroyed because the distance between them increases to 4 Å. (e) Comparison of MIDAS residues in the open conformation (aquamarine) and the closed conformation (yellow). (f) RGLG1^{EGTA} (violet) shows identify with RGLG1^{E378A} (yellow) suggests that RGLG1^{EGTA} also adopts closed conformation. (g) The open (aquamarine) and closed (yellow) conformations differ primarily in the orientation of the $\alpha 7$ helix. This helix is depicted as blue in the open conformation and red in the closed conformation. Residues involved in conformational changes are labeled. (For interpretation of the references to colour in this figure legend, the reader is referred to the web version of this article.)

between Ca^{2+} and the backbone oxygen of Q288 is facilitated by a 0.4 Å shift of Ca^{2+} from the position of Mg^{2+} (Fig. 5a and b). Other coordinating residues for Ca^{2+} are the same as those of Mg^{2+} (Fig. 5c and d). A Ca^{2+} ion was assigned at this position in accordance with the following observations. First, Ca^{2+} is the only metal ion in the crystallization buffer. Second, the average distance between the metal ion and the coordinating ligands (2.42 Å) is close to Ca^{2+} . Third, Ca^{2+} preferentially forms a pentagonal bipyramidal rather than an octahedral coordination, whereas Mg^{2+} and Mn^{2+} preferentially form an octahedral coordination,

and Mg^{2+}/Mn^{2+} does not form coordinate bonds with backbone oxygen atoms. Therefore, the typical pentagonal bipyramidal and backbone oxygen coordination distinguish the ion from Mg^{2+}/Mn^{2+} . Hypothesis that a high Ca^{2+} concentration might result in a competition with Mg^{2+}/Mn^{2+} and inhibit substrate binding has been proposed. However, some studies disagree with this hypothesis because Ca^{2+} is too large to bind MIDAS [12,29,30]. Our data show that the MIDAS of the RGLG1 VWA domain can be occupied by Ca^{2+} in the open conformation, inducing minimal global structural changes. And, RGLG1- Ca^{2+} showed a different coordination with

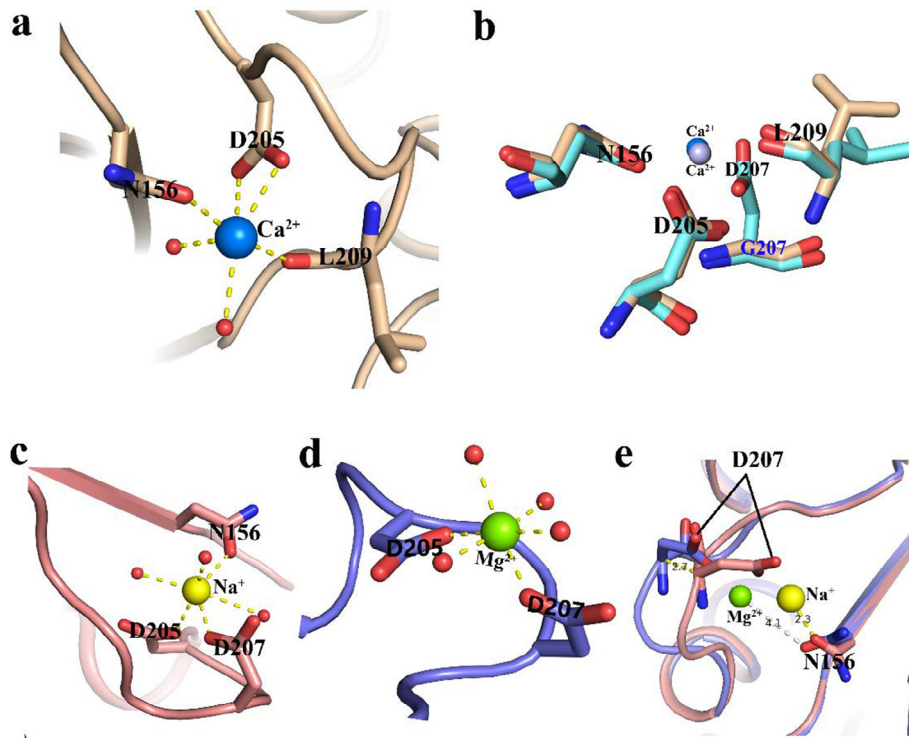


Fig. 4. The novel Ca^{2+} binding site 2 (NCBS2). (a) In the RGLG1^{D207G} crystal structure, a Ca^{2+} (marine) ion occupies the NCBS2 and adopts an octahedral coordination. It is coordinated by two water molecules, D205, N156, and L209. (b) In RGLG1^{D207G} (wheat), D207G mutation prevents G207 from coordinating with Ca^{2+} (blue), but there is no rearrangement of other residues compared to RGLG1¹²⁹ (aquamarine). (c) In the closed conformation (except for RGLG1^{D338A}), NCBS2 is occupied by Na^{+} (yellow). Na^{+} is coordinated by three water molecules, D205, D207 and N156. (d) In the crystal structure of RGLG1^{D338A}, Mg^{2+} (chartreuse) in NCBS2 is coordinated by D205, D207 and four water molecules. (e) In RGLG1^{E378A} (salmon), the distance between Na^{+} (a yellow sphere) and N156 is 2.3 Å. In RGLG1^{D338A} (light blue), Mg^{2+} (a chartreuse sphere) tends to move away from N156, and coordination is broken due to the distance between them exceeded 4 Å. (For interpretation of the references to colour in this figure legend, the reader is referred to the web version of this article.)

Ca^{2+} than those reported previously for Ca^{2+} -bound VWA domains [13,19]. In addition, RGLG1- Ca^{2+} binds the pseudo ligand in the open conformation; however, most Ca^{2+} -bound VWA domains adopt the closed conformation, and the rest are unliganded.

2.6. Open-closed conformation transition independent of Mg^{2+}

An open conformation was observed (RGLG1^{open}- H_2O) with MIDAS occupied by a water molecule. Although the H_2O -E153 distance increased to 3.1 Å, E153 of neighboring molecules is still sufficient to coordinate RGLG1^{open}- H_2O as a pseudo ligand at least under non-physiological crystallization conditions (Fig. 6a). This is the first ion-free ligand-bound open conformation of VWA domains. In ion-free-MIDAS in C2a- Li^{+} , the side chain of S244 (equivalent to S166 in RGLG1) was rotated by approximately 90° to compensate for the loss of charge [31]. In the disulfide-engineered α L I domain, D239 (equivalent to D286 in RGLG1) rotates distally to compensate for the loss of charge [32]. In our structures, superposition of RGLG1¹²⁹ with RGLG1¹²⁹- H_2O shows a virtually identical conformation in the side chain of S166, D286, and all other MIDAS residues (Fig. 6b and c). In addition, the ion-free closed conformation (RGLG1^{closed}- H_2O) (Fig. 6d) also shows only minor rearrangements in comparison with RGLG1^{E378A} (Fig. 6e).

This study shows that the state of RGLG1 VWA is not influenced by Mg^{2+} occupancy in MIDAS, since MIDAS can be occupied by a Mg^{2+} ion or a water molecule, and these structures display an identical state, concurrent with previous findings that Mg^{2+} is not sufficient to induce an open state [33].

2.7. Molecular dynamics simulations of affinity between RGLG1 and PP2CA

Previous results support the fact that conformations of the integrin I domains regulate the ligand binding potential, with the closed and open conformations corresponding to low and high affinity, respectively [32]. Unfortunately, a complete ligand-bound RGLG1 complex was not obtained; hence, the affinity remains mystery. Since PP2CA is a central negative regulator in the ABA signaling network and a substrate of RGLG1, it can be used to evaluate the affinity of RGLG1 in different conformations through MD simulations. Binding free energy (ΔG_{bind}) was determined to evaluate their energetic aspects. The ΔG_{bind} values of the open state and closed state of RGLG1/PP2CA were -101.97 and -89.17 kcal mol⁻¹, respectively (Table 3). As expected, the results of MD simulations suggest that the open state has much higher ligand affinity than the closed state. According to the energy components of the binding free energy (see Eqs. (2) and (3)), electrostatic interaction (ΔE_{ele}) is pivotal for the affinity of RGLG1/PP2CA. In addition, van der Waals interaction (ΔE_{vdw}) also played a role to enhance the stability of the system. However, these values are obtained through simulations and further evidences will be required to validate them.

3. Discussion

RGLG1, as a critical regulator in apical dominance and the ABA signaling pathway, has been evaluated via biochemical, immunological, and cell biological approaches [1,4]. Our study shows

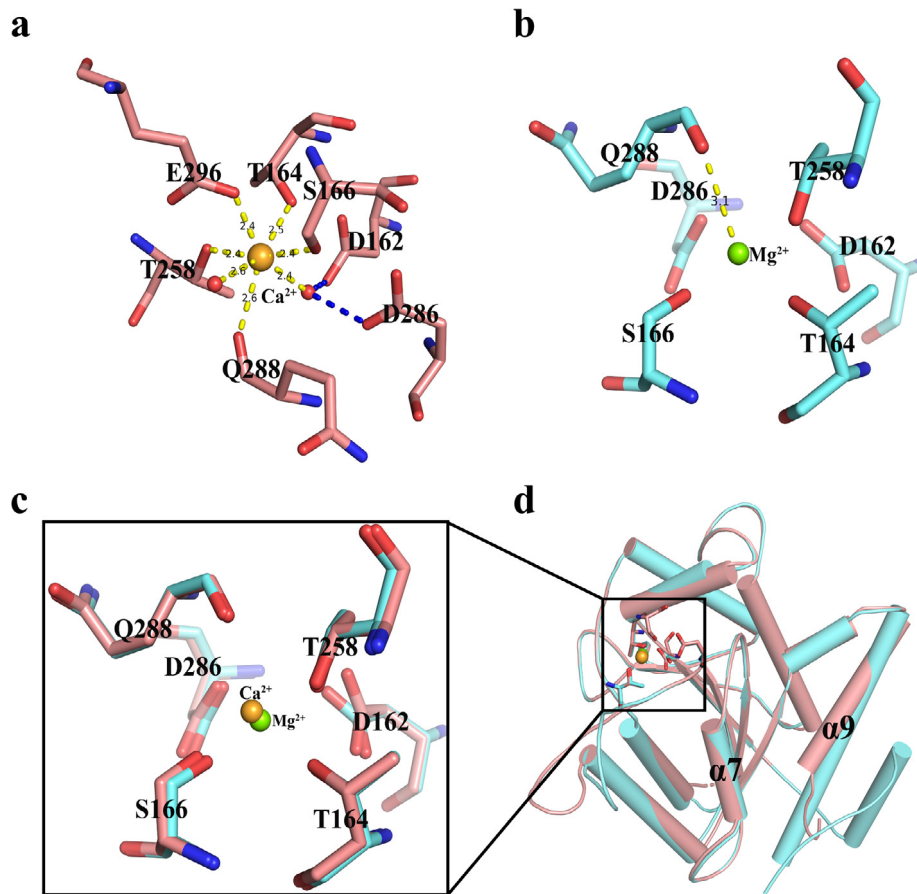


Fig. 5. Structure of Ca^{2+} binding MIDAS. (a) In the RGLG1- Ca^{2+} structure, Ca^{2+} (brightorange sphere) in MIDAS is coordinated by E296 from adjacent domain, S166, T164, T258, Q288, and two water molecules. The blue dotted lines represent hydrogen bonds. (b) In RGLG1¹²⁹, Q288 is too far away from Mg^{2+} (3.1 Å) to coordinate it. (c) Expansion of (d) around MIDAS. The ligand for Ca^{2+} (brightorange sphere) in RGLG1- Ca^{2+} is identical to that of Mg^{2+} (chartreuse sphere) in RGLG1¹²⁹, except for Q288. However, there is no significant shift in MIDAS residues. (d) The structure of RGLG1- Ca^{2+} (salmon) is superimposed onto the structure of the RGLG1¹²⁹ (aquamarine). (For interpretation of the references to colour in this figure legend, the reader is referred to the web version of this article.)

that the conformations of the RGLG1 VWA domain are Ca^{2+} -dependent. All structures of RGLG1 VWA adopt a typical Rossmann fold without the anti-parallel β sheet normally present in VWA, with sheet topology 21345 rather than the common sheet topology 321456. Sheet topology 21345 has not been discovered in VWA domains, whereas cutinases, a serine esterase, possesses similar sheet topology [34]. In integrin α I domains, the C-terminal helix and the preceding loop allosterically cause conformational switches in MIDAS [32]. In RGLG1 VWA, its conversion is independent of the movement of the C-terminal helix. Moreover, two novel Ca^{2+} binding sites (NCBS1 and NCBS2) are present, and through structure-guided mutagenesis experiments, we prove that the shift in conformation is clearly dependent on the occupancy of Ca^{2+} at NCBS1. Thus far, in all VWA domains, only integrin I domains have revealed a paradigm of conformational change [26]. Notably, the RGLG1 structures provide novel insights into the Ca^{2+} -based allosteric switch and conformational changes. After binding Ca^{2+} , the deflection of $\alpha 7$ disrupts the interaction between 286D and Mg^{2+} , and the movement of Mg^{2+} ion allows it to be coordinated by 258T. The pseudo ligand completes the coordination, then the conformation is changed to the open state. The only effect of mutations at D338 and E378 for RGLG1, whether single or double mutation, is inhibiting Ca^{2+} binding. It's worth noting that the allosteric regulator for the RGLG1 VWA domain is Ca^{2+} ions, not mutations. Mutations at key residues in NCBS1 only cause the corresponding allosteric switches through inhibiting Ca^{2+} binding. This result is proved by the structure of RGLG1^{EGTA}, which is crys-

tallized in the closed conformation with 2 mM EGTA supplemented in the purification buffer to eliminate calcium ions, avoiding any mutations.

Our findings are consistent with Belda-Palazon et al., who have proposed that ABA and calcium ions promote nuclear localization of the RGLG1 [7]. We speculate that ABA treatment may induce calcium-based allosteric switch of RGLG1 and convert RGLG1 to open state due to ABA can lead to increased Ca^{2+} levels. As we all known, ABA and calcium signaling processes are integrated and interconnected [35], therefore, the effect of ABA may be achieved through Ca^{2+} ions. In vitro, RGLG1 adopt the open state that can directly bind ligands, which can explain why ABA is not required for the interaction in vitro. Structural comparison of RGLG1 open state and closed state shows that a significant change occurs in the N-terminal $\alpha 1$, and during RGLG1 shuttle to the nucleus, specific plant proteases might catalyze the hydrolysis of N-myristoylated glycine residues [7]. Thus, we hypothesize that the movement of the $\alpha 1$ can cause variable in N-terminal region, allowing RGLG1 to bind to the specific proteases, and facilitating its shuttling and interaction with its target.

To investigate the effect of Ca^{2+} on the structural dynamics of NCBS1 residues, referring to Espinoza-Fonseca et al. [36], we performed four independent MD simulations based on the crystal structure of RGLG1¹²⁹ and RGLG1^{EGTA}, starting with the presence or absence of initially-bound Ca^{2+} . All simulations were performed for 100 ns. We plotted time-dependent distance evolution of the carboxyl-carboxyl or carboxyl-acylamino pairs between key resi-

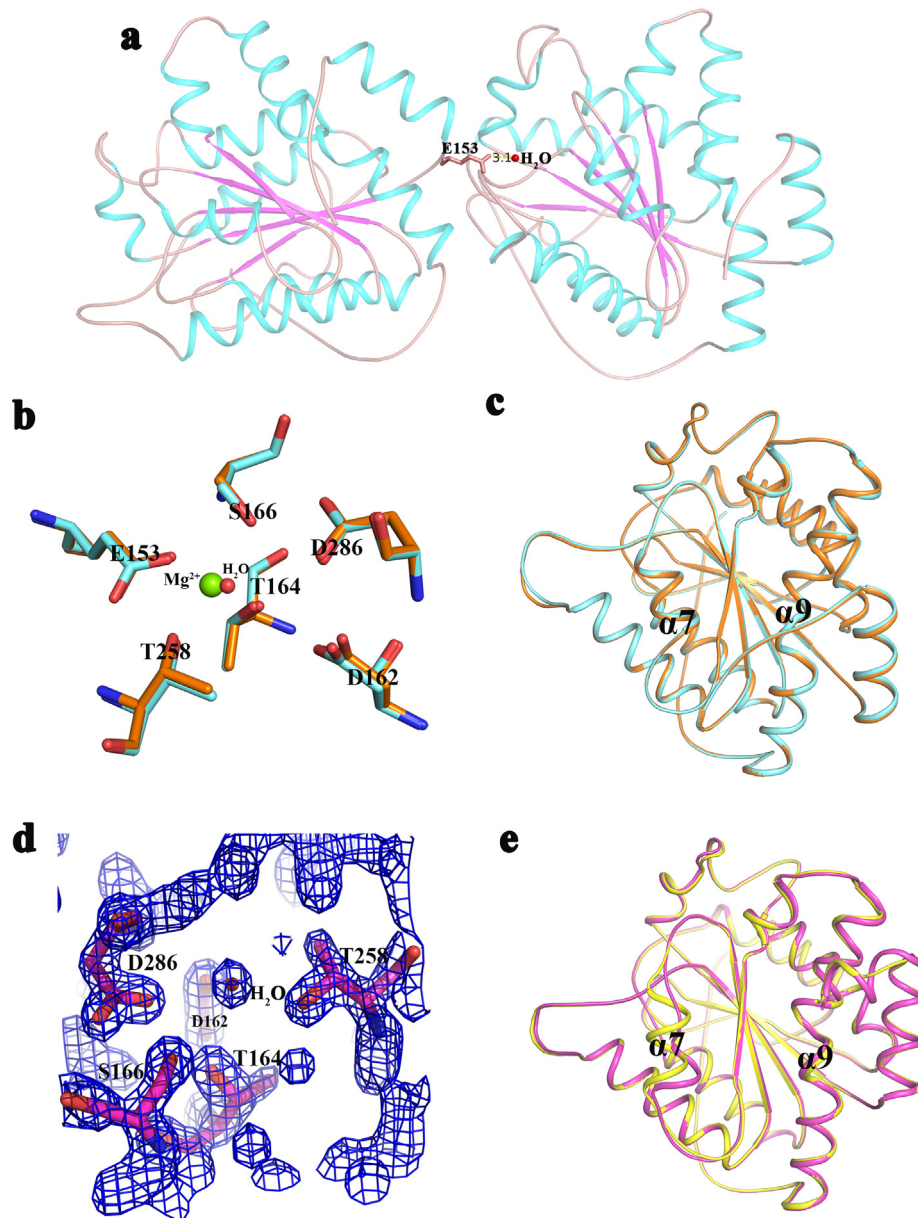


Fig. 6. Ion-free-MIDAS. (a) RGLG1¹²⁹-H₂O adopts pseudo-liganded conformation. A crystal asymmetric unit contains two molecules. H₂O-E153 distance increased to 3.1 Å. Water is shown as a small red sphere. (b) The MIDAS motif of RGLG1¹²⁹ (aquamarine) and RGLG1¹²⁹-H₂O (orange). No rearrangements are observed in MIDAS residues. Mg²⁺ ion in RGLG1¹²⁹ is depicted by a chartreuse sphere, and a water molecular in RGLG1¹²⁹-H₂O is shown as a small red sphere. (c) Structure of RGLG1¹²⁹ (aquamarine) and RGLG1¹²⁹-H₂O (orange) are compared. They are nearly identical. (d) The electron density of ion-free-MIDAS in the closed conformation. MIDAS residues are shown in magenta. In this structure, Mg²⁺ is replaced by a water molecule (small red sphere). (e) The structure of RGLG1^{E378A} (yellow) and RGLG1^{closed}-H₂O (magenta) are compared. (For interpretation of the references to colour in this figure legend, the reader is referred to the web version of this article.)

dues D338, E378, D347 and Q350 in the 100 ns-long MD simulations. Starting from the RGLG1¹²⁹ crystal structure, we found that the Ca²⁺ ion remained binding to NCBS1 during the entire 100 ns simulation (Fig. 8 and Supplementary Fig. 2). In Ca²⁺-free-RGLG1¹²⁹ (the crystal structure of RGLG1¹²⁹ but removing Ca²⁺), the distances of D338-E378, D338-Q350 and D347-E378 are larger compared to that of RGLG1¹²⁹, with an upward trend. Interestingly, the distance between D338 and D347 had large fluctuation during 30 ns–50 ns time scale, and finally went down to a similar distance scale of RGLG1^{EGTA} (Fig. 8). All distances in Ca²⁺-free-RGLG1¹²⁹ are similar to RGLG1^{EGTA}, calculated from the RGLG1^{EGTA} crystal structure, indicating that Ca²⁺-free-RGLG1¹²⁹ can convert to closed state (Fig. 8). Furthermore, new trajectory was performed using the final frame of 100 ns production run of the Ca²⁺-free-RGLG1¹²⁹ as start-

ing configuration, as expected, Ca²⁺ induced conformation change to closed state (Fig. 8). Dependent on the analyses of the MD trajectories, we propose that VWA domain can maintain open state in the presence of initially-bound Ca²⁺, otherwise it adopts the closed state. These studies provide detailed insights on Ca²⁺ binding and allosteric coupling of domain dynamics. Furthermore, we calculated the interdomain distance distributions of Ca²⁺-free-RGLG1¹²⁹, RGLG1¹²⁹, RGLG1^{EGTA} and RGLG1¹²⁹-con to analyze the structural dynamics using C α -C α distance of L140-D338. The atom-pair distance distributions fit very well to an either one or two Gaussian distribution (Fig. 9). Noticeably, two peaks were both found in Ca²⁺-free-RGLG1¹²⁹ and RGLG1¹²⁹-con, corresponding to the open and closed conformations. These results show that Ca²⁺ ions control the dynamic equilibrium of structural ensembles.

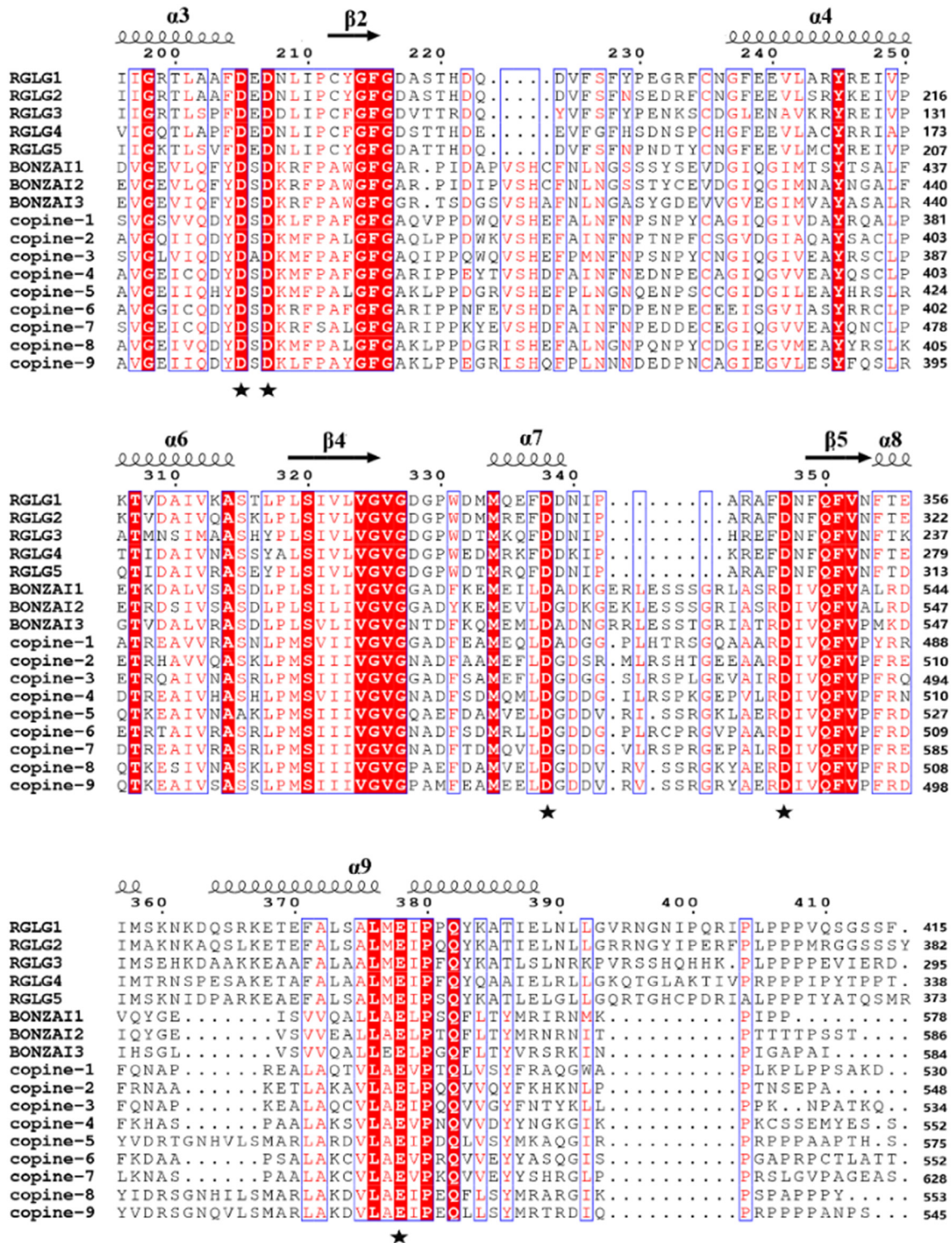


Fig. 7. Sequence alignment of the calcium binding sites between RGLG family and copines. The sequences were aligned with CLUSTALW. BONZAI1-3 are three copines family members from *Arabidopsis Thaliana*. Copine1-9 are nine copines family members from *Homo sapiens*. Key residues in NCBS1 and NCBS2 (D205, D207, D338, D347, and E378) are marked with black pentacles. All key residues are highly conserved in RGLG family, *Homo sapiens* copines family and *Arabidopsis thaliana* copines family.

Sequence alignment of RGLG1 using ClustalW revealed that copines and other RGLG family members share high sequence identity with RGLG1 at the VWA domain. Copines are phospholipid-binding proteins with three family members in *Arabidopsis thaliana* and nine orthologues in *Homo sapiens*. Each copine

contains two N-terminal C2 domains followed by a C-terminal VWA domain in both *Homo sapiens* and *Arabidopsis thaliana*. The C2 domains can response to the increases of intracellular calcium levels to bind to the phospholipid. In *Arabidopsis thaliana*, copines play important role in growth regulation and disease resistance

Table 3
Binding free energy (ΔG_{bind}) calculated for RGLG1/PP2CA complexes (units in kcal mol⁻¹).

	ΔE_{ele}	ΔE_{vdw}	ΔE_{psol}	ΔE_{pbele}	ΔG_{bind}
RGLG1 ¹²⁹	-299.44 ± 42.04	-107.99 ± 7.37	305.4 ± 35.99	17.60 ± 11.62	-101.97 ± 6.49
RGLG1 ^{EGTA}	-228.21 ± 23.75	-91.63 ± 6.50	228.69 ± 21.62	11.95 ± 3.67	-91.15 ± 3.20
RGLG1 ^{D338A}	-184.20 ± 39.14	-104.91 ± 5.68	192.99 ± 30.58	20.93 ± 9.84	-96.11 ± 4.11
RGLG1 ^{E378A}	-201.53 ± 28.60	-84.96 ± 7.31	208.24 ± 33.40	16.39 ± 5.81	-78.25 ± 2.67
RGLG1 ^{D338A/E378A}	-230.24 ± 18.04	-91.30 ± 6.67	230.38 ± 18.76	10.64 ± 4.93	-91.16 ± 2.27

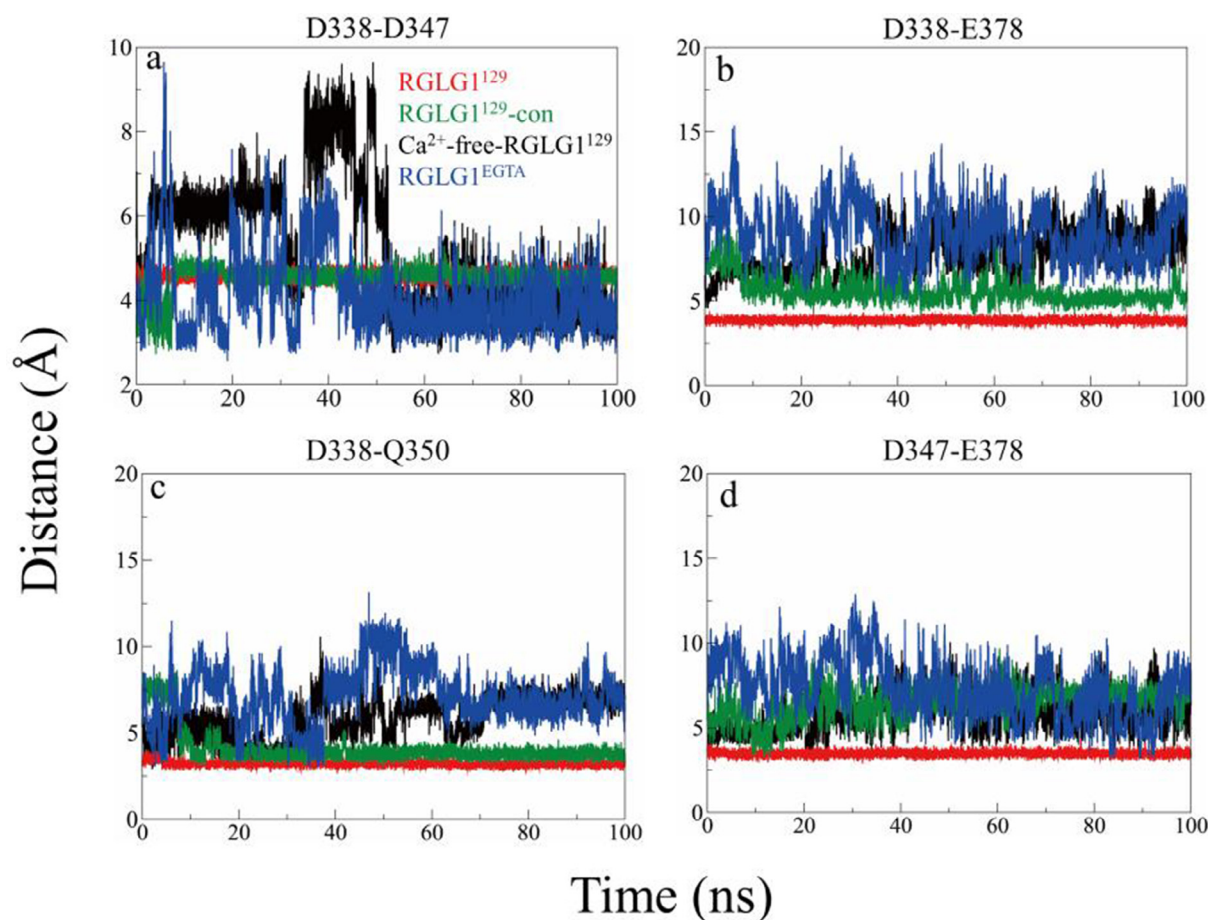


Fig. 8. Time-dependent distance evolution of carboxyl-carboxyl or carboxyl-acylamino pairs between residues D338, E378, D347 and Q350. Distances were calculated for MD simulations from the crystal structures of RGLG1 (RGLG1¹²⁹, RGLG1¹²⁹-con, Ca²⁺-free-RGLG1¹²⁹ and RGLG1^{EGTA}).

[37]. In *Homo sapiens*, most copines are expressed ubiquitously and are primarily involved in membrane trafficking of intracellular signaling proteins [38]. Further comparison of copines with RGLG1 on key residues (D205, D207, D338, D347, and E378) in NCBS1/2 reveals that these residues are highly conserved in copines (Fig. 7). It is hypothesized that these copines may also contain the two novel Ca²⁺ binding sites (NCBS1/2) and their conformational changes depend on Ca²⁺ as well, thus facilitating further examination of the structural and functional properties of copines. Our structures potentially provide a suitable paradigm for future studies investigating novel mechanisms for other VWA proteins.

Usually, MIDAS binding divalent cations are required for ligand binding in the VWA domains [10,33]. However, RGLG1-H₂O binds the pseudo ligand without a divalent cation, and conformation is identical to that of RGLG1¹²⁹, wherein MIDAS is occupied by Mg²⁺, probably because the divalent cation is required for initial ligand binding, and subsequent movement of ion to produce a metal-free VWA domain-ligand complex. The conjecture has been proposed in integrin-ligand complex [39].

Ca²⁺ serves as an allosteric regulator for the RGLG1 VWA domain has been determined in this paper. Previous studies have shown that open state represents high affinity in integrin VWA domain. According to the results of our MD simulation, open state of RGLG1 VWA also represent higher affinity. In other words, after binding Ca²⁺, RGLG1 VWA can bind its ligand, e.g., PP2CA, thereafter, the ABA signaling pathway may be activated upon PP2CA degradation through RGLG1. However, the mechanism of calcium-mediated protein interactions *in vivo* is still unknown, thus, future studies are required.

4. Methods

4.1. Protein preparation and crystallization

RGLG1¹²⁹ and RGLG1-Ca²⁺ was cloned into a bacterial expression vector PET32a to generate a fusion protein containing a 6his tag, an N-terminal Trx tag, and a TEV cleavage site between the 6his tag and the target protein. *E. coli* BL21 cells were transformed

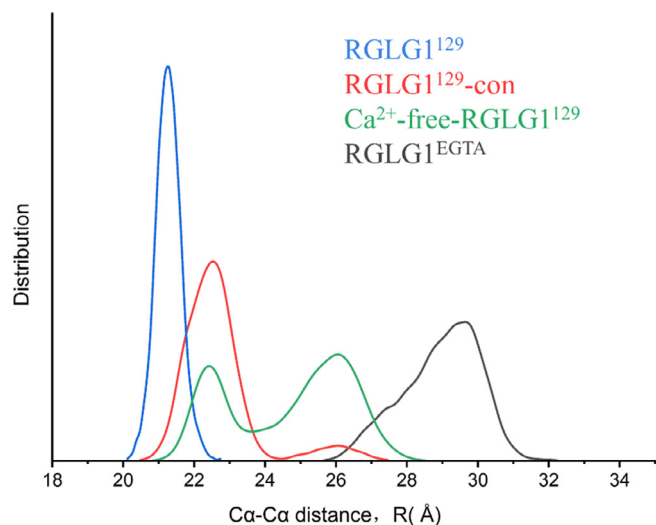


Fig. 9. Distance distributions between L140-D338 of RGLG. MD trajectories of Ca^{2+} -free-RGLG1¹²⁹ (green), RGLG1¹²⁹ (blue), RGLG1^{EGTA} (black) and RGLG1¹²⁹-con (red) were used to calculate Ca - Ca distance distribution between L140-D338. (For interpretation of the references to colour in this figure legend, the reader is referred to the web version of this article.)

with the expression vector, and cells were cultured in 1 L LB medium up to an A_{600} of 0.4–0.6 at 37 °C and induced with isopropyl- β -D-1-thiogalactopyranoside (IPTG) at 0.3 mM at 16 °C for 14 h. Cells were then harvested at 6000 rpm for 5 min at 16 °C, resuspended in 30 ml lysis buffer (300 mM NaCl, 50 mM Tris-HCl pH 8.0, 5% glycerol, 20 mM imidazole, and 1% [w/v] Tween). After sonication, insoluble material was eliminated via centrifugation at 20,000 rpm for 20 min at 4 °C, and the supernatant was applied to a Ni-NTA column. The column was washed with 150 ml lysis buffer and eluted with elution buffer (300 mM NaCl, 50 mM Tris-HCl pH 8.0, 5% glycerol, and 300 mM imidazole). The eluted fusion protein was dialyzed and cleaved overnight with TEV protease in lysis buffer without 20 mM imidazole. The cleaved protein was separated from the His tag and TEV protease, using a Ni-NTA column. Target proteins were further purified via size-exclusion chromatography (SEC, Superdex-200, GE Healthcare) in buffer A (150 mM NaCl, 25 mM Tris-HCl pH 8.0, and 5% glycerol). Mutants were purified with the aforementioned method, except that buffer A was supplemented with 2 mM EGTA during RGLG1^{EGTA} purification.

All protein crystals were grown at 16 °C via the sitting-drop vapor diffusion method containing 0.5 μ l of purified protein at 7 mg/ml and 0.5 μ l of reservoir solution. Optimal crystallization conditions are depicted in [Supplementary Table S1](#).

4.2. Data collection, structure determination, and refinement

Before data collection, all crystals were briefly soaked with cryoprotectant and flash-frozen in liquid nitrogen. X-ray diffraction data were obtained at Shanghai Synchrotron Radiation Facility (SSRF), processed with HKL2000 package or Xia2. RGLG1¹²⁹ phases were obtained via single-wavelength anomalous scattering experiments and analyzed using PHENIX AutoSol. Other structures were resolved using RGLG1¹²⁹ as the molecular replacement model in PHASER. Further refinements were carried out using PHENIX and manual model construction in Coot.

4.3. Molecular dynamics simulation

The initial configurations of the RGLG1 and PP2CA system for Molecule dynamics (MD) simulations were generated using ZDOCK

3.0.2 [40]. MD simulations were carried out using GROMACS-2018.3, with the AMBER ff99SB-ILDN force field [41,42]. The protonation states of protein residues were assigned using PROPKA web-server on the basis of predicted pKa values [43]. All systems were explicitly solvated with TIP3P water molecules in 9 Å buffer and neutralized with counter ions. The particle mesh Ewald (PME) algorithm [44] was used to determine long-range electrostatic energies, and van der Waals and Coulomb interactions were truncated at 10 Å. All bond lengths were constrained using the LINCS algorithm.

The systems were subjected to 2500 steps of steepest-descent and 2500 steps of conjugate-gradient minimization to eliminate poor interatomic contacts. The system was first gradually heated from 0 K to 298 K and then equilibrated for 500 ps at 1 atm in an isochoric/isothermal (NPT) ensemble with periodic boundary conditions. Temperature and pressure controls were achieved using Nosé-Hoover thermostat and Berendsen barostat with a frequency of 2.0 ps, respectively [45,46]. Finally, 150 ns-long MD simulations were carried out with each system. The most representative structures were identified via cluster analysis.

4.4. Binding free energies

The molecular mechanics Poisson Boltzmann solvent accessible surface area (MM/PBSA) approach was successfully applied to predict the binding free energy (ΔG_{bind}) in various protein–ligand or protein–protein complexes [47–49]. Here, three parallel MD simulations of each system were carried out and the first 100 snRGLG1hots were extracted from each MD trajectory of each complex. Computational details were as follows:

$$\Delta G_{\text{bind}} = \Delta H - T\Delta S \approx \Delta E_{\text{gas}} + \Delta G_{\text{sol}} - T\Delta S \quad (1)$$

$$\Delta E_{\text{gas}} = \Delta E_{\text{ele}} + \Delta E_{\text{vdW}} \quad (2)$$

$$\Delta G_{\text{sol}} = \Delta G_{\text{pol}} + \Delta G_{\text{np}} \quad (3)$$

where ΔE_{gas} , ΔG_{sol} and $-T\Delta S$ represent the changes in binding energy in the gaseous phase, solvation, and the conformational entropy upon binding, respectively. ΔE_{gas} included ΔE_{ele} (electrostatic) + ΔE_{vdW} (van der Waals) potential. ΔG_{sol} included contributions of polar (ΔG_{pol}) and nonpolar (ΔG_{np}) terms. Since the binding conformational entropy (ΔS) was computationally expensive and poorly accurate, we assumed that ΔG_{bind} was approximately equal to the sum of ΔE_{gas} and ΔG_{sol} .

CRedit authorship contribution statement

Qin Wang: Investigation, Writing - original draft, Writing - review & editing, Conceptualization, Methodology, Visualization, Formal analysis. **YaYu Chen:** Software, Methodology. **ShengPing Li:** Resources. **WenDi Yang:** Writing - review & editing. **LiFang Sun:** Methodology, Funding acquisition. **MeiQin Jang:** Methodology. **Xiuling Wu:** Methodology. **QianChao Wang:** Methodology. **Lifei Chen:** Methodology. **Yunkun Wu:** Supervision, Funding acquisition.

Declaration of Competing Interest

The authors declare that they have no known competing financial interests or personal relationships that could have appeared to influence the work reported in this paper.

Acknowledgments

The authors thank Shanghai Synchrotron Radiation Facility (SSRF) for access to the beamlines BL19U1, BL18U1 and BL17U1 and the beamline staff for assistance with diffraction data collection. This work was supported by the Key Project of Fujian Province (2017N0031), the STS project of Chinese Academy of Sciences and Fujian Province (2016T3041), the National Nature Science Foundation of China (31470741), Special Funds of the Central Government Guiding Local Science and Technology Development (2017L3009), National Thousand Talents Program of China, Postdoctoral Science Foundation of China (2016M592096) and Nature Science Foundation of Fujian Province (2016J01173).

Appendix A. Supplementary data

Supplementary data to this article can be found online at <https://doi.org/10.1016/j.csbj.2020.03.023>.

References

- [1] Yin XJ et al. Ubiquitin lysine 63 chain forming ligases regulate apical dominance in Arabidopsis. *Plant Cell* 2007;19(6):1898–911. <https://doi.org/10.1105/tpc.107.052035>.
- [2] Li W, Schmidt W. A lysine-63-linked ubiquitin chain-forming conjugase, UBC13, promotes the developmental responses to iron deficiency in Arabidopsis roots. *Plant J* 2010;62(2):330–43. <https://doi.org/10.1111/j.1365-3113.2010.04150.x>.
- [3] Pan IC, Schmidt W. Functional implications of K63-linked ubiquitination in the iron deficiency response of Arabidopsis roots. *Front Plant Sci* 2014;4. <https://doi.org/10.3389/fpls.2013.00542>.
- [4] Wu Q et al. Ubiquitin ligases RGLG1 and RGLG5 regulate abscisic acid signaling by controlling the turnover of phosphatase PP2CA. *Plant Cell* 2016;28(9):2178–96. <https://doi.org/10.1105/tpc.16.00364>.
- [5] Cutler SR, Rodriguez PL, Finkelstein RR, Abrams SR. Abscisic acid: emergence of a core signaling network. *Annu Rev Plant Biol* 2010;61:651–79. <https://doi.org/10.1146/annurev-arplant-042809-112122>.
- [6] Umezawa T et al. Type 2C protein phosphatases directly regulate abscisic acid-activated protein kinases in Arabidopsis. *Proc Natl Acad Sci* 2009;106(41):17588–93. <https://doi.org/10.1073/pnas.0907095106>.
- [7] Belda-Palazon B et al. ABA inhibits myristoylation and induces shuttling of the RGLG1 E3 ligase to promote nuclear degradation of PP2CA. *Plant J* 2019;98(5):813–25. <https://doi.org/10.1111/tpj.14274>.
- [8] Whittaker CA, Hynes RO, Pollard TD. Distribution and evolution of von willebrand/integrin A domains: widely dispersed domains with roles in cell adhesion and elsewhere. *Mol Biol Cell* 2002;13(10):3369–87. <https://doi.org/10.1091/mbc.e02-05-0259>.
- [9] Becker AK, Mikolajek H, Paulsson M, Wagener R, Werner JM. A structure of a collagen VI VWA domain displays N and C termini at opposite sides of the protein. *Structure (London, England: 1993)* 2014;22(2):199–208. <https://doi.org/10.1016/j.str.2013.06.028>.
- [10] Luo BH, Carman CV, Springer TA. Structural basis of integrin regulation and signaling. *Annu Rev Immunol* 2007;25:619–47. <https://doi.org/10.1146/annurev.immunol.25.022106.141618>.
- [11] Lee JO, Bankston LA, Arnaout MA, Liddington RC. Two conformations of the integrin A-domain (I-domain): a pathway for activation?. *Structure (London, England: 1993)* 1995;3(12):1333–40.
- [12] Lee JO, Rieu P, Arnaout MA, Liddington R. Crystal structure of the A domain from the alpha subunit of integrin CR3 (CD11b/CD18). *Cell* 1995;80(4):631–8.
- [13] Shimaoka M et al. Reversibly locking a protein fold in an active conformation with a disulfide bond: Integrin I domains with high affinity and antagonist activity in vivo. *Proc Natl Acad Sci* 2001;98(11):6009–14. <https://doi.org/10.1073/pnas.101130498>.
- [14] Mould AP et al. Conformational changes in the integrin beta A domain provide a mechanism for signal transduction via hybrid domain movement. *J Biol Chem* 2003;278(19):17028–35. <https://doi.org/10.1074/jbc.M213139200>.
- [15] Xiao T, Takagi J, Collier BS, Wang J-H, Springer TA. Structural basis for allostery in integrins and binding to fibrinogen-mimetic therapeutics. *Nature* 2004;432(7013):59–67. <https://doi.org/10.1038/nature02976>.
- [16] Zhang K, Chen J. The regulation of integrin function by divalent cations. *Cell Adhesion Migration* 2012;6(1):20–9. <https://doi.org/10.4161/cam.18702>.
- [17] Bhattacharya AA, Lupher ML, Staunton DE, Liddington RC. Crystal structure of the A domain from complement factor B reveals an integrin-like open conformation. *Structure (London, England: 1993)* 2004;12(3):371–8. <https://doi.org/10.1016/j.str.2004.02.012>.
- [18] Chen J, Salas A, Springer TA. Bistable regulation of integrin adhesiveness by a bipolar metal ion cluster. *Nat Struct Mol Biol* 2003;10(12):995–1001. <https://doi.org/10.1038/nsb1011>.
- [19] Mould AP, Barton SJ, Askari JA, Craig SE, Humphries MJ. Role of ADMIDAS cation-binding site in ligand recognition by integrin alpha5beta1. *J Biol Chem* 2003;278(51):51622–9. <https://doi.org/10.1074/jbc.M306655200>.
- [20] Leitinger B, McDowall A, Stanley P, Hogg N. The regulation of integrin function by Ca(2+). *BBA* 2000;1498(2–3):91–8.
- [21] Xiong JP. Crystal structure of the extracellular segment of integrin alpha Vbeta 3. *Science (New York, N.Y.)* 2001;294(5541):339–45. <https://doi.org/10.1126/science.1064535>.
- [22] Xiong JP et al. Crystal structure of the extracellular segment of integrin alpha Vbeta3 in complex with an Arg-Gly-Asp ligand. *Science (New York, N.Y.)* 2002;296(5565):151–5. <https://doi.org/10.1126/science.1069040>.
- [23] Harding MM. The geometry of metal-ligand interactions relevant to proteins. II. Angles at the metal atom, additional weak metal-donor interactions. *Acta Crystallogr D Biol Crystallogr* 2000;56(Pt 7):857–67.
- [24] Harding MM. The geometry of metal-ligand interactions relevant to proteins. *Acta Crystallogr D Biol Crystallogr* 1999;55(Pt 8):1432–43.
- [25] Lacy DB, Wigelsworth DJ, Scobie HM, Young JAT, Collier RJ. Crystal structure of the von Willebrand factor A domain of human capillary morphogenesis protein 2: an anthrax toxin receptor. *Proc Natl Acad Sci* 2004;101(17):6367–72. <https://doi.org/10.1073/pnas.0401506101>.
- [26] Springer TA. Complement and the multifaceted functions of VWA and integrin I domains. *Structure (London, England: 1993)* 2006;14(11):1611–6. <https://doi.org/10.1016/j.str.2006.10.001>.
- [27] Emsley J, Cruz M, Handin R, Liddington R. Crystal structure of the von Willebrand factor A1 domain and implications for the binding of platelet glycoprotein Ib. *J Biol Chem* 1998;273(17):10396–401.
- [28] Xia W, Springer TA. Metal ion and ligand binding of integrin alpha5beta1. *Proc Natl Acad Sci* 2014;111(50):17863–8. <https://doi.org/10.1073/pnas.1420645111>.
- [29] Emsley J, Knight CG, Farndale RW, Barnes MJ, Liddington RC. Structural basis of collagen recognition by integrin alpha2beta1. *Cell* 2000;101(1):47–56. [https://doi.org/10.1016/s0092-8674\(00\)80622-4](https://doi.org/10.1016/s0092-8674(00)80622-4).
- [30] Onley DJ, Knight CG, Tuckwell DS, Barnes MJ, Farndale RW. Micromolar Ca2+ concentrations are essential for Mg2+-dependent binding of collagen by the integrin alpha2beta1 in human platelets. *J Biol Chem* 2000;275(32):24560–4. <https://doi.org/10.1074/jbc.M00411200>.
- [31] Milder FJ et al. Structure of complement component C2a: implications for convertase formation and substrate binding. *Structure (London, England: 1993)* 2006;14(10):1587–97. <https://doi.org/10.1016/j.str.2006.08.008>.
- [32] Shimaoka M et al. Structures of the alpha L I domain and its complex with ICAM-1 reveal a shape-shifting pathway for integrin regulation. *Cell* 2003;112(1):99–111.
- [33] Qu A, Leahy DJ. The role of the divalent cation in the structure of the I domain from the CD11a/CD18 integrin. *Structure (London, England: 1993)* 1996 4(8), 931–942.
- [34] Medvedev KE, Kinch LN, Grishin NV. Functional and evolutionary analysis of viral proteins containing a Rossmann-like fold. *Protein Sci* 2018;27(8):1450–63. <https://doi.org/10.1002/pro.3438>.
- [35] Edel KH, Kudla J. Integration of calcium and ABA signaling. *Curr Opin Plant Biol* 2016;33:83–91. <https://doi.org/10.1016/j.pbi.2016.06.010>.
- [36] Espinoza-Fonseca LM, Autry JM, Thomas DD. Microsecond molecular dynamics simulations of Mg(2+)- and K(+)-bound E1 intermediate states of the calcium pump. *PLoS ONE* 2014;9(4):. <https://doi.org/10.1371/journal.pone.0095979>.
- [37] Jambunathan N, Siani JM, McNellis TW. A humidity-sensitive Arabidopsis copine mutant exhibits precocious cell death and increased disease resistance. *Plant Cell* 2001;13(10):2225–40.
- [38] Creutz CE et al. The copines, a novel class of C2 domain-containing, calcium-dependent, phospholipid-binding proteins conserved from Paramecium to humans. *J Biol Chem* 1998;273(3):1393–402.
- [39] Dickeson SK, Bhattacharyya-Pakrasi M, Mathis NL, Schlesinger PH, Santoro SA. Ligand binding results in divalent cation displacement from the alpha 2 beta 1 integrin I domain: evidence from terbium luminescence spectroscopy. *Biochemistry* 1998;37(32):11280–8. <https://doi.org/10.1021/bi9727848>.
- [40] Pierce BG, Hourai Y, Weng Z. Accelerating protein docking in ZDOCK using an advanced 3D convolution library. *PLoS ONE* 2011;6(9):. <https://doi.org/10.1371/journal.pone.0024657>.
- [41] Hess B, Kutzner C, van der Spoel D, Lindahl E. GROMACS 4: algorithms for highly efficient, load-balanced, and scalable molecular simulation. *J Chem Theory Comput* 2008;4(3):435–47. <https://doi.org/10.1021/ct700301q>.
- [42] Lindorff-Larsen K et al. Systematic validation of protein force fields against experimental data. *PLoS ONE* 2012;7(2):. <https://doi.org/10.1371/journal.pone.0032131>.
- [43] Olsson MH, Sondergaard CR, Rostkowski M, Jensen JH. PROPKA3: consistent treatment of internal and surface residues in empirical pKa predictions. *J Chem Theory Comput* 2011;7(2):525–37. <https://doi.org/10.1021/ct100578z>.
- [44] Kholmurodov K, Smith W, Yasuoka K, Darden TA, Ebisuzaki T. A smooth-particle Mesh Ewald method for DL_POLY molecular dynamics simulation package on the Fujitsu VPP700. *J Comput Chem* 2000;21(13):1187–91.
- [45] Hoover WG. Canonical dynamics: equilibrium phase-space distributions. *Phys Rev A, General Phys* 1985;31(3):1695–7.

- [46] Berendsen HJC, Postma JPM, Van Gunsteren WF, Dinola A, Haak JR. Molecular-dynamics with coupling to an external bath. *J Chem Phys* 1984;81(8):3684–90.
- [47] Hou T, Wang J, Li Y, Wang W. Assessing the performance of the MM/PBSA and MM/GBSA methods. 1. The accuracy of binding free energy calculations based on molecular dynamics simulations. *J Chem Inf Model* 2011;51(1):69–82. <https://doi.org/10.1021/ci100275a>.
- [48] Ileana S, Kashif S, Coveney PV. Rapid and accurate prediction of binding free energies for saquinavir-bound HIV-1 proteases. *J Am Chem Soc* 2008 130(8), 2639–2648.
- [49] Chen F et al. Assessing the performance of the MM/PBSA and MM/GBSA methods. 6. Capability to predict protein–protein binding free energies and re-rank binding poses generated by protein–protein docking. *PCCP* 2016;18(32):22129–39.